Journal of
Mechanics of
Materials and Structures

NONLINEAR DYNAMIC CHARACTERISTICS OF A VIBRO-IMPACT SYSTEM UNDER HARMONIC EXCITATION

Jianlian Cheng and Hui Xu

Volume 1, Nº 2 February 2006

mathematical sciences publishers

JOURNAL OF MECHANICS OF MATERIALS AND STRUCTURES
Vol. 1, No. 2, 2006

NONLINEAR DYNAMIC CHARACTERISTICS OF A VIBRO-IMPACT SYSTEM UNDER HARMONIC EXCITATION

JIANLIAN CHENG AND HUI XU

Dynamical behaviors of a two-degree-of-freedom (TDOF) vibro-impact system are investigated. The theoretical solution of periodic-one double-impact motion is obtained by differential equations, periodicity and matching conditions, and the Poincaré map is established. The dynamics of the system are studied with special attention to Hopf bifurcations of the impact system in nonresonance, weak resonance, and strong resonance cases. The Hopf bifurcation theory of maps in $\mathbb{R}^2$-strong resonance is applied to reveal the existence of Hopf bifurcations of the system. The theoretical analyses are verified by numerical solutions. The evolution from periodic impacts to chaos in nonresonance, weak resonance, and strong resonance cases, is obtained by numerical simulations. The results show that dynamical behavior of the system in the strong resonance case is more complicated than that of the nonresonance and weak resonance cases.

1. Introduction

An impact damper is basically a small free mass within a main mass with clearances between the moving masses. Impact dampers in various forms have been used successfully for controlling high-amplitude vibration systems in many practical applications, such as in cutting tools, turbine blades and tall flexible structures like chimneys [Ema and Marui 1996; Cheng and Wang 2003; Wang et al. 2003; Dimentberg and Iourtchenko 2004; Chatterjee and Mallik 1995]. If an impact damper is properly designed, the vibration system structure can be effectively simplified and its performance will be less sensitive to the changes of the system parameters, as compared to a conventional dynamic vibration damper. The vibration of the primary system is controlled by the transfer of momentum to a secondary mass through repeated impacts. Impacts occur when the amplitudes of vibration of the system exceed critical values. Investigation of vibro-impact problems is of significance to the optimization design of machinery with clearances or gaps, and to reliability analysis and noise suppression. Since systems

Keywords: Hopf bifurcation, strong resonance, quasiperiodic motion, vibro-impact, chaos.
The authors gratefully acknowledge the support of the National Science Foundation of China (No. 10372076).

with impact dampers are strongly nonlinear and discontinuous due to the existence of one or more impact pairs of components, the vibro-systems can show very rich and complicated dynamic behavior. In recent years, vibro-impact problems have become a new subject in nonlinear dynamics. Subjects of recent research include singularity [Chatterjee and Mallik 1996; Whiston 1992]; inelastic vibro-impacts [Luo et al. 2001]; high codimension bifurcation [Wen 2001; Luo and Xie 2003; Xie and Ding 2005]; Hopf bifurcations [Padmanabhan and Singh 1995; Luo and Chen 2005; Ding et al. 2004; Luo 2004a]; and quasiperiodic impacts [Blazejczyk-Okolewska 2001; Luo 2004b; Cone and Zadoks 1995]; and so on. Dynamics and bifurcations of a class of single-degree-of-freedom self-excited oscillators with an impact damper were studied by Chatterjee and Mallik [1995]. Cone and Zadoks [1995] investigated the nonlinear behavior of an impact oscillator with the addition of dry friction. The periodic solutions were interpreted by using bifurcation theory and the nonlinear behavior of this system was identified as a function of both the excitation amplitude and the excitation frequency for the two levels of dry friction force. Many nonlinear dynamical behaviors including turning point bifurcations, symmetry breaking pitchfork bifurcations, period-doubling bifurcation cascades, and so on, were explained. Asfar and Akour [2005] studied the suppression of self-excited vibrations with an impact viscous damper and used the optimization method to determine the design parameters for suppressing self-excited vibrations.

In recent decades, nonsmooth dynamics of mechanical systems with impacts have been a focus of several investigations; many new results were obtained and a few new methods have been established. Holmes [1982] found small horseshoe maps in a mathematical model for the bouncing ball. The classical pattern of period-doubling bifurcation cascade was observed numerically by Shaw and Holmes [1983] and Thompson and Ghaffari [1982]. Recently, a few researchers have begun to focus on the quasiperiodic and chaotic motions of vibro-impact systems. Chatterjee and Mallik [1995] studied quasiperiodic vibro-impacts in a class of single-degree-of-freedom self-excited oscillators with an impact damper. Budd et al. [1995] studied vibro-impact of a single-degree-of-freedom system contacting a single stop and proved that if the coefficient of restitution is less than 1, quasiperiodic motion cannot occur in the system. Luo and Xie [2003] investigated codimension-2 bifurcations of a single-degree-of-freedom impact oscillator and found a Hopf bifurcation of a period-2 two-impact orbit. Xie and Ding [2005] studied Hopf bifurcations of a two-degree-of-freedom vibro-impact system in the strong resonance, nonresonance, and weak resonance cases, and analyzed the routes of quasiperiodic impacts to chaos. Nordmark [1991] investigated the nonperiodic motion caused by grazing bifurcation. The normal form mapping for such grazing phenomena was developed in [di Bernardo et al. 2001; 2002].

Therefore, a periodically forced, piecewise, linear system with impacts is of great interest.

In this paper, the impact damper system serves as a two-degree-of-freedom (TDOF) vibro-impact system with a proportional damping property. We focus our attention on Hopf bifurcation of period motions with one impact in the strong resonance, nonresonance or weak resonance cases. Stability and bifurcation conditions for periodic motion will be obtained. A Poincaré section of the vibro-impact system with proportional damping is chosen to establish the Poincaré map, and then periodic motion with one impact and the stability thereof are investigated by analytical methods. Numerical simulations of periodic and chaotic motions will be presented to validate the analytical results.

2. Mechanical model of the vibro-impact system

The mechanical model for a vibro-impact system with masses M_1 and M_2 is shown in Figure 1. The main mass M_1 is connected to the seat with a linear spring with stiffness K and a linear viscous dashpot of damping constant C. In this system, when the impact mass, or *free mass*, collides with the main mass during vibration, an impulsive force acts on both and produces transfer of momentum with loss of energy. Impact damping is used to simulate an inelastic collision with restitution coefficient $R < 1$. We neglect friction and the duration of the impact between the two masses.

The behavior of the system between any two consecutive impacts is considered. For convenience, the time t between any two consecutive impacts is always set to zero directly at the instant when the former impact is over, and the phase angle is used only to make a suitable choice for the origin of time in the calculation. Phase angle, velocities, and displacements of the system at that instant become initial conditions in the subsequent process of the motion. Between impacts, the differential equations of motion of the vibro-impact system are given by

$$M_1\ddot{X}_1 + C\dot{X}_1 + KX_1 = F_0 \sin(\Omega T + \varphi), \tag{1}$$

$$M_2\ddot{X}_2 = 0 \quad \text{whenever } |X_1 - X_2| < D/2, \tag{2}$$

where the dot denotes differentiation with respect to time T.

Substituting the nondimensional parameters

$$\begin{aligned} \omega_n &= \sqrt{K/M_1}, & \zeta &= n/\omega_n, \\ n &= C/2M_1, & \omega &= \Omega\sqrt{M_1/K}, \\ t &= T\sqrt{K/M_1}, & x_i &= KX_i/F_0 \quad (i = 1, 2), \\ \delta &= KD/2F_0, & \mu &= M_2/M_1 \end{aligned}$$

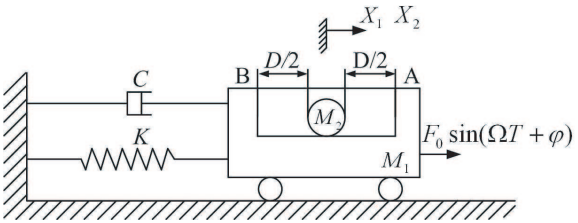

Figure 1. Schematic diagram of the impact system.

into Equations (1) and (2) yields

$$\ddot{x}_1 + 2\zeta\omega_n\dot{x}_1 + \omega_n^2 x_1 = \sin(\omega t + \varphi), \tag{3}$$

$$\ddot{x}_2 = 0 \quad \text{whenever } |x_1 - x_2| < \delta, \tag{4}$$

where the dot denotes differentiation with respect to dimensionless time t.

When $|x_1 - x_2| = \delta$, a collision occurs. According to the conservation law of momentum and the definition of the restitution coefficient, we can obtain

$$\dot{x}_{1+} + \mu\dot{x}_{2+} = \dot{x}_{1-} + \mu\dot{x}_{2-}, \tag{5}$$

$$\dot{x}_{2+} - \dot{x}_{1+} = R(\dot{x}_{1-} - \dot{x}_{2-}), \tag{6}$$

where $\dot{x}_{i-}$ and $\dot{x}_{i+}$ $(i = 1, 2)$ denotes respectively, the instantaneous velocities before and after impacts. By Equations (5) and (6), the departure velocities of the masses M_1 and M_2 after impact at the instant are given by

$$\begin{aligned} \dot{x}_{1+} &= \frac{1-\mu R}{1+\mu}\dot{x}_{1-} + \frac{\mu(1+R)}{1+\mu}\dot{x}_{2-}, \\ \dot{x}_{2+} &= \frac{1+R}{1+\mu}\dot{x}_{1-} + \frac{\mu-R}{1+\mu}\dot{x}_{2-}, \end{aligned} \tag{7}$$

where $\mu = M_2/M_1$.

The general solutions of Equations (3) and (4) are

$$\begin{cases} x_1(t) = e^{-\zeta\omega_n t}\big(a_{11}\cos(\eta\omega_n t) + b_{11}\sin(\eta\omega_n t)\big) + A\sin(\omega t + \tau), \\ x_2(t) = a_{12} + b_{12}t, \end{cases} \quad 0 \le t \le t_1, \tag{8a}$$

$$\begin{cases} x_1(t) = e^{-\zeta\omega_n(t-t_1)}\big(a_{21}\cos(\eta\omega_n(t-t_1)) + b_{21}\sin(\eta\omega_n(t-t_1))\big) \\ \qquad\qquad + A\sin(\omega t + \tau), \\ x_2(t) = a_{22} + b_{22}(t - t_1) \end{cases} \quad t_1 \le t \le t_p, \tag{8b}$$

where $t_p = t_1 + t_2$, t_1 and t_2 are the traveling time of the impact mass M_2 from $A \to B$ and $B \to A$ in the groove. The integration constants are

$$\eta = \sqrt{1-\zeta^2},$$
$$\gamma = \omega/\omega_n,$$
$$A = 1/\omega_n^2\left((1-\gamma^2)^2 + (2\zeta\gamma)^2\right)^{1/2},$$
$$\tau = \varphi - \psi 1,$$
$$\psi = \tan^{-1}(2\zeta\gamma/(1-\gamma^2)),$$
$$a_{ki} \text{ and } b_{ki} \quad (k = 1, 2).$$

3. Stability of periodic motion and Poincaré map

We choose a Poincaré section $\sigma \subset \mathbb{R}^4 \times S$, which is given by

$$\sigma = \left\{(x_1, \dot{x}_1, x_2, \dot{x}_2, \theta) \in R^4 \times S, \dot{x}_1 = \dot{x}_{1+}, \dot{x}_2 = \dot{x}_{2+}, x_2 - x_1 = \delta\right\}, \tag{9}$$

to establish a Poincaré map

$$X' = \tilde{f}(v, X), \tag{10}$$

where $\theta = \omega t$, $v \in R^1$ is a real parameter, $X = X^* + \Delta X$, $X' = X^* + \Delta X'$, $\Delta X = (\Delta\dot{x}_{1+}, \Delta x_{10}, \Delta\dot{x}_{2+}, \Delta\tau)^T$, $\Delta X' = (\Delta\dot{x}'_{1+}, \Delta x'_{10}, \Delta\dot{x}'_{2+}, \Delta\tau')^T$, ΔX and $\Delta X'$ are the disturbed vectors of $X^* \cdot X^* = (\dot{x}_{1+}, x_{10}, \dot{x}_{2+}, \tau)^T$ is a fixed point of periodic impacts in Poincaré section, which corresponds to one impact during one forcing cycle.

Under suitable system parameter conditions, the system given in Figure 1 can exhibit 1-1-1 symmetrical periodic motion. We can characterize periodic motions of the vibro-impact system by the symbol n-p-q, where p and q are the number of impacts occurring at the stops A and B, respectively, and n is the number of the forcing cycles. The periodic behavior means that if the dimensionless time t is set to zero directly after an impact, it becomes $2\pi/\omega$ just before the next impact between the masses M_1 and M_2 at point location A, where the mass M_2 come-and-go motion time t_1 and t_2 in the groove are equal to π/ω. After the origin of the θ-coordinate is displaced to an impact point, the determination is based on the fact that they satisfy the following set of periodicity and matching conditions

$$\begin{aligned}
x_i(0) &= -x_i(\pi/\omega) = x_{i0},\\
\dot{x}_i(2\pi/\omega) &= -\dot{x}_{i-}(\pi/\omega) = \dot{x}_{i-},\\
\dot{x}(0) &= -\dot{x}_{i+}(\pi/\omega) = \dot{x}_{i+},\\
x_2(0) - \dot{x}_1(0)i &= \delta,\\
x_2(\pi/\omega) - x_1(\pi/\omega) &= \delta,\\
x_2(2\pi/\omega) - x_1(2\pi/\omega) &= \delta.
\end{aligned} \tag{11}$$

Substituting the periodicity boundary condition Equation (11) into the general solution (8), we can solve for the integration constants a_{ki}, b_{ki} $(k, i = 1, 2)$ and the phase angle τ_0. We obtain

$$a_{k1} = (-1)^k m(\delta + A\sin\tau_0) \qquad a_{k2} = (-1)^{k+1}(1+m)(\delta + A\sin\tau_0), \tag{12}$$

$$b_{k1} = (-1)^{k+1}\pi mn(\delta + A\sin\tau_0) \qquad b_{k2} = (-1)^k d(1+m)(\delta + A\sin\tau_0), \tag{13}$$

$$\tau_0 = \arccos\frac{hq \pm h\sqrt{h^2 - h^2q^2 + 1}}{1+h^2}, \tag{14}$$

where

$$m = \frac{s\mu d e_1}{(e_1^2 + 2ce_1 + 1)\eta\omega_n - (se_1 d + ce_1 + 1)\mu}, \qquad d = \frac{2\omega}{\pi},$$

$$n = \frac{1+ce_1}{se_1}, \qquad e_1 = e^{-\pi\zeta/\gamma}, \qquad \gamma = \omega/\omega_n, \qquad s = \sin\eta\pi/\gamma,$$

$$c = \cos\eta\pi/\gamma, \qquad q = \delta/A,$$

$$h = \frac{(\mu - R)(\omega(1+2m) + \pi m(1+2ce_1)) + \pi mn(1+\mu)}{\pi\omega(1+R)} + \frac{2me_1(s\eta - c\zeta) - de_1 mn(s\zeta + c\eta)}{d\gamma}. \tag{15}$$

In Equation (14), "±" denotes that there may be two different 1-1-1 symmetrical periodic motions under uniform system parameters. Because $|\cos\tau_0| \le 1$, it should be noted that the existence of periodic impacts meets the condition

$$h^2 - h^2q^2 + 1 \ge 0, \qquad \left|\frac{hq \pm h\sqrt{h^2 - h^2q^2 + 1}}{1+h^2}\right| \le 1. \tag{16}$$

For expressing the actual motion of the system, the periodic solution must satisfy simultaneously the conditions of existence and stability. We consider the perturbed motion of 1-1-1 periodic motion to establish its Poincaré map. For simplicity of notations, the origin of the θ-coordinate is displaced to an impact point; the solutions of the perturbed motion are written in the form

$$\begin{cases} \tilde{x}_1(t) = e^{-\zeta\omega_n t}\left(\tilde{a}_{11}\cos(\eta\omega_n t) + \tilde{b}_{11}\sin(\eta\omega_n t)\right) \\ \qquad\qquad + A\sin(\omega t + \tau_0 + \Delta\tau), \quad 0 \le t \le \tilde{t}_1, \\ \tilde{x}_2(t) = \tilde{a}_{12} + \tilde{b}_{12}t \end{cases} \tag{17a}$$

$$\begin{cases} \tilde{x}_1(t) = e^{-\zeta\omega_n(t-t_1)}\left(\tilde{a}_{21}\cos(\eta\omega_n(t-\tilde{t}_1)) + \tilde{b}_{21}\sin(\eta\omega_n(t-\tilde{t}_1))\right) \\ \qquad\qquad + A\sin(\omega t + \tau_0 + \Delta\tau), \quad \tilde{t}_1 \le t \le \tilde{t}_p, \\ \tilde{x}_2(t) = \tilde{a}_{22} + \tilde{b}_{22}(t - \tilde{t}_1) \end{cases} \tag{17b}$$

For the disturbed motion, the dimensionless time is set to zero directly after an impact at point A between the masses M_1 and M_2. It becomes $(2\pi + \Delta\theta)/\omega$ just before the next impact at the same point, and the boundary conditions at two successive impact points are given by

$$\begin{aligned}
\tilde{x}_i(0) &= x_{i0} + \Delta x_{i0}, & \dot{\tilde{x}}_i(0) &= \dot{x}_{i+} + \Delta\dot{x}_{i+},\\
\tilde{x}_i(\tilde{t}_1) &= -x_{i0} + \Delta x'_{i0}, & \dot{\tilde{x}}_{i-}(\tilde{t}_1) &= -\dot{x}_{i-} + \Delta\dot{x}'_{i-},\\
\dot{\tilde{x}}_{i+}(\tilde{t}_1) &= -\dot{x}_{i+} + \Delta\dot{x}'_{i+}, & \tilde{x}_i(\tilde{t}_p) &= x_{i0} + \Delta x''_{i0},\\
\dot{\tilde{x}}_{i-}(\tilde{t}_p) &= \dot{x}_{i-} + \Delta\dot{x}''_{i-}, & \dot{\tilde{x}}_{i+}(\tilde{t}_p) &= \dot{x}_{i+} + \Delta\dot{x}''_{i+},
\end{aligned}$$

$$\begin{aligned}
(\dot{x}_{2+} + \Delta\dot{x}_{2+})\tilde{t}_1 + 2x_{10} + \Delta x_{10} - \Delta x'_{10} &= -2\delta,\\
(-\dot{x}_{2+} + \Delta\dot{x}'_{2+})(\tilde{t}_p - \tilde{t}_1) - 2x_{10} + \Delta x'_{10} - \Delta x''_{10} &= 2\delta\\
\Delta\theta = \omega(\Delta t_1 - \Delta t_2),&
\end{aligned} \tag{18}$$

where $\tilde{t}_1 = \pi/\omega + \Delta t_1$, $\tilde{t}_2 = \pi/\omega + \Delta t_2$.

Substituting the boundary condition Equation (12) into Equations (17a) and (17b), we obtain

$$\begin{aligned}
\tilde{a}_{11} &= x_{10} + \Delta x_{10} - A\sin(\tau_0 + \Delta\tau),\\
\tilde{a}_{21} &= -x_{10} + \Delta x'_{10} - A\sin(\omega\tilde{t}_1 + \tau_0 + \Delta\tau),\\
\tilde{a}_{12} &= x_{20} + \Delta x_{20}, \qquad \tilde{a}_{22} = -x_{20} + \Delta x'_{20}, \qquad \tilde{b}_{12} = \dot{x}_{2+} + \Delta x_{2+},\\
\tilde{b}_{22} &= -\dot{x}_{2+} + \Delta\dot{x}'_{2+},\\
\tilde{b}_{11} &= \dot{x}_{1+} + \Delta\dot{x}_{1+} - A\omega\cos(\tau_0 + \Delta\tau) + \zeta\omega_n\sin(\tau_0 + \Delta\tau)\\
&\quad + \zeta\omega_n(x_{10} + \Delta x_{10})/\eta\omega_n,\\
\tilde{b}_{21} &= \left[\begin{array}{l} -\dot{x}_{1+} + \Delta\dot{x}'_{1+} - A\omega\cos(\omega\tilde{t}_1 + \tau_0 + \Delta\tau)\\ \quad - \zeta\omega_n A\sin(\omega\tilde{t}_1 + \tau_0 + \Delta\tau) - \zeta\omega_n(x_{10} - \Delta x'_{10}) \end{array}\right] \Big/ \eta\omega_n.
\end{aligned} \tag{19}$$

If we substitute the boundary condition Equation (18) into the perturbed solution (Equations (17a) and (17b)) for $t = t_e$, we obtain

$$\begin{aligned}
\Delta x'_{10} &= \tilde{x}_1(t_e) - x_{10},\\
\Delta\dot{x}'_{1+} &= \frac{\mu(1+R)}{1+\mu}\dot{\tilde{x}}_1(t_e) + \frac{1-\mu R}{1+\mu}\dot{\tilde{x}}_{2+}(t_e) - \dot{x}_{1+},\\
\Delta\dot{x}'_{2+} &= \frac{\mu - R}{1+\mu}\dot{\tilde{x}}_1(t_e) + \frac{1+R}{1+\mu}\dot{\tilde{x}}_2(t_e) - \dot{x}_{2+},\\
\Delta\tau' &= \Delta\tau + \Delta\theta.
\end{aligned} \tag{20}$$

Define a function $w(\Delta\dot{x}_{1+}, \Delta x_{10}, \Delta\dot{x}_{2+}, \Delta\tau, \Delta t_1)$ as

$$w(\Delta\dot{x}_{1+}, \Delta x_{10}, \Delta\dot{x}_{2+}, \Delta\tau, \Delta t_1) \stackrel{\text{def}}{=} \tilde{x}_2(\tilde{t}_1) - \tilde{x}_1(\tilde{t}_1) + \delta = 0. \tag{21}$$

Assuming $\partial w/\partial \Delta t_1|_{(0,0,0,0)} \neq 0$, according to the implicit function theorem, Equation (21) can be solved as

$$\Delta t_1 = \Delta t_1(\Delta\dot{x}_{1+}, \Delta x_{10}, \Delta\dot{x}_{2+}, \Delta\tau).$$

Setting

$$\Delta X = (\Delta\dot{x}_{1+}, \Delta x_{10}, \Delta\dot{x}_{2+}, \Delta\tau)^T = (y_1, y_2, y_3, y_4)^T,$$

we deduce the partial differentials of Δt_1 with respect to $\Delta\dot{x}_{1+}$, Δx_{10}, $\Delta\dot{x}_{2+}$ and $\Delta\tau$, as follows:

$$\frac{\partial \Delta t_1}{\partial y_j} = -\frac{\partial w}{\partial y_j} \Big/ \frac{\partial w}{\partial \Delta t_1}, \quad j = 1, 2, 3, 4. \tag{22}$$

In the same way, we define a function

$$h(\Delta\dot{x}_{1+}, \Delta x_{10}, \Delta\dot{x}_{2+}, \Delta\tau, \Delta t_1, \Delta t_2) \stackrel{\text{def}}{=} \tilde{x}_2(t_p) - \tilde{x}_1(t_p) - \delta = 0 \tag{23}$$

By supposing $\partial h/\partial \Delta t_2|_{(0,0,0,0)} \neq 0$, based on the implicit function theorem, we have

$$\frac{\partial \Delta t_2}{\partial y_j} = -\left(\frac{\partial h}{\partial y_j} + \frac{\partial h}{\partial \Delta t_1}\frac{\partial \Delta t_1}{\partial y_j}\right) \Big/ \frac{\partial h}{\partial \Delta t_2}. \tag{24}$$

According to this analysis, we then obtain the Poincaré map, which is given by

$$\begin{aligned}
\Delta\dot{x}'_{1+} &= \tilde{f}_1(\Delta\dot{x}_{1+}, \Delta x_{10}, \Delta\dot{x}_{2+}, \Delta\tau, \Delta\theta) - \dot{x}_{1+} \stackrel{\text{def}}{=} f_1(\Delta\dot{x}_{1+}, \Delta x_{10}, \Delta\dot{x}_{2+}, \Delta\tau),\\
\Delta\dot{x}'_{10} &= \tilde{f}_2(\Delta\dot{x}_{1+}, \Delta x_{10}, \Delta\dot{x}_{2+}, \Delta\tau, \Delta\theta) - x_{10} \stackrel{\text{def}}{=} f_2(\Delta\dot{x}_{1+}, \Delta x_{10}, \Delta\dot{x}_{2+}, \Delta\tau),\\
\Delta\dot{x}'_{2+} &= \tilde{f}_3(\Delta\dot{x}_{1+}, \Delta x_{10}, \Delta\dot{x}_{2+}, \Delta\tau, \Delta\theta) - \dot{x}_{2+} \stackrel{\text{def}}{=} f_3(\Delta\dot{x}_{1+}, \Delta x_{10}, \Delta\dot{x}_{2+}, \Delta\tau),\\
\Delta\tau' &= \Delta\tau + \Delta\theta(\Delta\dot{x}_{1+}, \Delta x_{10}, \Delta\dot{x}_{2+}, \Delta\tau) \stackrel{\text{def}}{=} f_4(\Delta\dot{x}_{1+}, \Delta x_{10}, \Delta\dot{x}_{2+}, \Delta\tau).
\end{aligned} \tag{25}$$

Letting $v = \omega$, the Poincaré map Equation (25) can be expressed as

$$\Delta X' = \tilde{f}(v, X) - X^* \stackrel{\text{def}}{=} f(v, \Delta X), \tag{26}$$

in which

$$\begin{aligned}
f(v, \Delta X) &= (f_1, f_2, f_3, f_4)^T,\\
\Delta X &= (\Delta\dot{x}_{1+}, \Delta x_{10}, \Delta\dot{x}_{2+}, \Delta\tau)^T,\\
\Delta X' &= (\Delta\dot{x}'_{1+}, \Delta x'_{10}, \Delta\dot{x}'_{2+}, \Delta\tau')^T.
\end{aligned}$$

We expand the function $f(v, \Delta X)$ as a Taylor series in the variables ΔX and v, so that it becomes

$$f(v, \Delta X) = \sum_{p+q \geq 1} F_{pq} v^p \Delta X^q, \tag{27}$$

$$F_{pq} = \frac{1}{p!q!} \frac{\partial^{p+q} f(v, \Delta X)}{\partial v^p \partial X^q}\bigg|_{(v_c,0)}, \qquad F_{p0} \equiv 0, \ \ p \geq 1, \tag{28}$$

$$f(v, \Delta X) = F_{01}\Delta X + vF_{11}\Delta X + v^2 F_{21}\Delta X + F_{02}[\Delta X^2] + F_{03}[\Delta X^3] + \cdots, \tag{29}$$

where F_{02} and F_{03} denote the second-order and the third-order terms respectively.

Linearizing the Poincaré map at the fixed point $X^* = (\dot{x}_{1+}, x_{10}, \dot{x}_{2+}, \tau)^T$ results in the matrix

$$Df(v, 0) = \begin{bmatrix} \frac{\partial f_1}{\partial \Delta \dot{x}_{1+}} & \frac{\partial f_1}{\partial \Delta x_{10}} & \frac{\partial f_1}{\partial \Delta \dot{x}_{2+}} & \frac{\partial f_1}{\partial \Delta \tau} \\ \frac{\partial f_2}{\partial \Delta \dot{x}_{1+}} & \frac{\partial f_2}{\partial \Delta x_{10}} & \frac{\partial f_3}{\partial \Delta \dot{x}_{2+}} & \frac{\partial f_4}{\partial \Delta \tau} \\ \frac{\partial f_3}{\partial \Delta \dot{x}_{1+}} & \frac{\partial f_3}{\partial \Delta x_{10}} & \frac{\partial f_3}{\partial \Delta \dot{x}_{2+}} & \frac{\partial f_3}{\partial \Delta \tau} \\ \frac{\partial f_4}{\partial \Delta \dot{x}_{1+}} & \frac{\partial f_4}{\partial \Delta x_{10}} & \frac{\partial f_4}{\partial \Delta \dot{x}_{2+}} & \frac{\partial f_4}{\partial \Delta \tau} \end{bmatrix}_{(v,0,0,0,0)}. \tag{30}$$

According to Equations (21) and (23), it is easy to calculate the derivatives in the matrix Equation (30):

$$\frac{\partial f_j}{\partial y_i} = \frac{\partial \tilde{f}_j}{\partial y_i} + \frac{\partial \tilde{f}_j}{\partial \Delta t_1}\frac{\partial \Delta t_1}{\partial y_i} + \frac{\partial \tilde{f}_j}{\partial \Delta t_2}\frac{\partial \Delta t_2}{\partial y_i} \quad i, j = 1, 2, 3, 4. \tag{31}$$

It is possible to determine the stability of periodic impacts by the eigenvalues of $Df(v, 0)$. If all eigenvalues of $Df(v, 0)$ are inside the unit circle, then the periodic solution is stable; otherwise, it is unstable. If some of the eigenvalues of the matrix $Df(v, 0)$ lie on the unit circle in the complex plane when $v = v_c$ (v_c is the bifurcation value), then it is possible for bifurcations to take place. In general, bifurcation occurs in various ways according to the number of the eigenvalues on the unit circle and their position on the circle. When $v = v_c$, $Df(v, 0)$ has a pair of simple complex conjugate eigenvalues $\lambda_1(v_c)$ and $\bar{\lambda}_1(v_c)$ on the unit circle; all other eigenvalues of $Df(v, 0)$ are inside the unit circle. Under this circumstance, 1-1-1 symmetrical periodic motion may lead to Hopf bifurcation. In general, bifurcations from periodic motions to quasiperiodic ones occur under nonresonance or resonance conditions in nonlinear dynamical systems.

4. Hopf bifurcation in nonresonance and weak resonance cases

Consider the Poincaré map

$$\Delta X' = f(v, \Delta X). \tag{32}$$

Let $\Delta X^*(v)$ be a fixed point for the system Equation (32) for v in some neighborhood of a critical value $v = v_c$ at which $Df(v, 0)$ satisfies the following assumptions:

(A1) $Df(v, 0)$ has a pair of complex conjugate eigenvalues

$$\lambda_1 = \lambda_1(v_c) \quad \text{and} \quad \lambda_2 = \bar{\lambda}_2(v_c),$$

and satisfies $|\lambda_1(v_c)| = 1$. The other eigenvalues $\lambda_i(v_c)$ satisfy

$$|\lambda_i(v_c)| < 1, \quad i = 3, 4;$$

(A2) $(d|\lambda_1(v_c)|dv)|_{v=v_c} > 0$;

(A3) $\lambda_1^m(v_c) \neq 1, \quad m = 1, 2, 3, 4.$

Let k_i denote the eigenvector of $Df(v, 0)$ corresponding to $\lambda_i(v)$, for $i = 1, 2, 3, 4$. If k_3 and k_4 are a complex conjugate pair of nonreal eigenvectors, define

$$H = (\operatorname{Re} k_1, -\operatorname{Im} k_1, \operatorname{Re} k_3, -\operatorname{Im} k_3);$$

otherwise,

$$H = (\operatorname{Re} k_1, -\operatorname{Im} k_1, k_3, k_4).$$

In some neighborhood of v_c, the map Equation (32), under the change of variable

$$\Delta X = HY, \qquad \mu = v - v_c, \tag{33}$$

becomes

$$Y' = F(\mu, Y), \tag{34}$$

where $Y = (y_1, y_2, y_3, y_4)^T$.

For the map Equation (34), there exists a local center manifold $W(z, \bar{z}; \mu)$, on which the local behavior of the map can be reduced to a two-dimensional map $\Phi_\mu(z)$. This map can be presented

$$\Phi_\mu(z) = \lambda(\mu)z + \sum_{i+j=2}^{3} g_{ij}(\mu)\frac{z^i \bar{z}^j}{i!j!} + O(|z|^4), \tag{35}$$

where $\lambda(\mu) = \lambda_1(v_c + \mu)$, $\lambda_0 = \lambda(0)$, $z = y_1 + iy_2$, $\bar{z} = y_1 - iy_2$.

By center manifold theory, all bifurcation phenomena of $F(\mu, Y)$ take place on a two-dimensional manifold. Local dynamic behavior of the map Equation (34) is equivalent to that of the two-dimensional map Equation (35) for μ in some

neighborhood of a critical value $\mu = 0$, so using the map Equation (35) and applying the following lemma, we can discuss the existence of Hopf bifurcation for map Equation (32) as v passes through v_c.

Lemma 1 [Lanford 1973; Wan 1978]. *Let $\Phi_\mu(z)$ be a one-parameter family of diffeomorphisms on R^2 near $z = 0$, satisfying the following conditions*:

(B1) $\Phi_\mu(0) = 0$ *for all* μ;

(B2) $D\Phi_\mu(0)$ *has two conjugate eigenvalues* $\lambda(\mu)$ *and* $\bar{\lambda}(\mu)$, *with* $|\lambda(0)| = 1$;

(B3) $(d|\lambda(\mu)|/d\mu)|_{\mu=0} > 0$;

(B4) $\lambda^m(0) \neq 1,\ m = 1, 2, 3, 4$.

Subject to assumptions (B1)–(B4), we can make a smooth μ-dependent change of coordinates to put $\Phi_\mu(z)$ into the normal form

$$\Phi_\mu(z) = N\Phi_\mu(z) + O(|Y|^5). \tag{36}$$

In polar co-ordinates,

$$N\Phi_\mu(r, \varphi) = (|\lambda(\mu)|r - f_1(\mu)r^3, \varphi + \theta(\mu) + f_3(\mu)r^3). \tag{37}$$

If $f_1(0) > 0$ (or $f_1(0) < 0$), $\Phi_\mu(z)$ has an attracting (repelling) invariant circle for $\mu > 0$ (or $\mu < 0$). Suppose that the complex form of $\Phi_0(z)$ is

$$\Phi_0(z) = \lambda_0 z + \sum_{i+j=2}^{3} g_{ij}(0)\frac{z^i \bar{z}^j}{i!j!} + O(|z|^4). \tag{38}$$

Then, there is

$$f_1(0) = \mathrm{Re}\left(\frac{(1-2\lambda_0)\bar{\lambda}_0}{2(1-\lambda_0)} g_{20}\, g_{11}\right) + \tfrac{1}{2}|g_{11}|^2 + \tfrac{1}{4}|g_{02}|^2 - \mathrm{Re}\,\frac{\bar{\lambda}_0 g_{21}}{2}, \tag{39}$$

where $\lambda_0 = \lambda(0)$, $g_{ij}(\mu)(i + j = 2, 3)$ (see the Appendix).

If the Poincaré map Equation (32) satisfies the conditions (A1)–(A3), then it is easy to show that the map Equation (35) satisfies the conditions (B1)–(B4). If a set of system parameters can be chosen for the vibro-impact system under which the Poincaré map Equation (32) satisfies the conditions (A1)–(A3), then by computing $f_1(0)$, we can conclude the existence of an invariant circle for the map Equation (35) and its stability in terms of the sign of $f_1(0)$. Because on the centre manifold $W(z, \bar{z}; \mu)$ the local behavior of the Poincaré map can be reduced to the two-dimensional behavior of Equation (35), it is certain that if the map Equation (35) has an attracting (repelling) invariant circle for $\mu > 0$ (or $\mu < 0$), a supercritical (subcritical) Hopf bifurcation will take place for the vibro-impact system shown in Figure 1 at $v = v_c$.

5. Numerical simulation of Hopf bifurcation and chaos for the vibro-impact system

In this section, the analyses developed in the previous section are verified by the numerical results for the impact system in Figure 1. The results of numerical simulations are used to understand the rich dynamical behavior that our model vibro-impact system exhibits. The use of these properties of chaotic systems can offer special advantages in controlling chaotic systems. For instance, small perturbations can lead to large effects, and flexible switching is possible between many different periodic orbits without changing the global configuration of the system. Many feedback control strategies based on this general idea use small perturbations in a control parameter to manipulate the behavior of chaotic systems. These benefits cannot be achieved in nonchaotic systems in which large effects in behavior typically require large changes in the control parameter.

Dynamic behavior of the vibro-impact system is shown in the projected Poincaré sections. The Poincaré section is taken in the form $\Sigma = \{(x_1, \dot{x}_1, x_2, \dot{x}_2, \theta) \in \mathbb{R}^4 \times S,\ \dot{x}_1 = \dot{x}_{1+}, \dot{x}_2 = \dot{x}_{2+}, x_2 - x_1 = \delta\}$, which is four-dimensional. The section is then projected onto the $(x_1, \dot{x}_1)$ plane, which is called the projected Poincaré section. Dynamic behavior of the vibro-impact system near the resonance point can be demonstrated from those projected Poincaré sections.

5.1. ***Hopf bifurcation to chaotic motion in nonresonance and weak resonance cases.*** Here we briefly analyze Hopf bifurcation to quasiperiodic torus and the break of quasiperiodic torus to chaotic behavior of the model in nonresonance and weak resonance cases. A set of parameters $\mu = 0.1$, $\omega_n = 0.5$, $\zeta = 0.045$, $R = 0.8$, $\delta = 5.0$ are considered. ω is taken as the control parameter, i.e. let $v = \omega$. The eigenvalues of $Df(\omega, 0)$ are computed for $\omega \in [0.5, 1.5]$. A pair of complex conjugate eigenvalues intersects the unit circle and the other eigenvalues are still inside the unit circle as ω passes through $\omega_c = 0.99176$. ω_c is a Hopf bifurcation value, at which $\lambda_{1,2}(\omega_c) = 0.2730961 \pm 0.9619876i$, $\lambda_{3,4}(\omega_c) = 0.3047823 \pm 0.2773642i$, and $|\lambda_{1,2}(\omega_c)| = 1$, $\lambda^m_{1,2}(\omega_c) \neq 1$, $m = 1, 2, 3, 4$. It is apparent that the model with this set of system parameters satisfies a nonresonance or weak resonance condition at the critical point. When $\omega \in (1.015, 1.45)$, the system can exhibit stable symmetry 1-1-1 periodic motion. When $\omega = 1.2$, the impact system exhibits stable periodic 1-1-1 impact motion; see Figure 2(a). Figure 2(b,c) show that the impact system exhibits unstable periodic motion, but in this case invariant circle is not generated. Taking a theoretical fixed point of the system corresponding to $\omega = 1.00857$ as an initial map point, the attracting invariant circle is shown in Figure 2(d,e,f). When the value of ω moves further away from the Hopf bifurcation value, the invariant circle, in projected Poincaré sections, expands markedly; see Figure 2(g,h). With further reduction in the control parameter ω, the attracting

invariant circle is broken; see Figure 2(i,j) and gets locked into a periodic attractor of higher period (higher than one cycle of the forcing). Subsequently, the system becomes unstable and chaotic. The periodic attractors of higher period, via phase locking (that is, the vibration frequencies of the oscillation system are locked in various rational multiples of the forcing frequency), is shown for $\omega = 0.9817$ in Figure 2(k). The chaotic motion of the system, represented by an infinite point set on a nonclosed curve in the projected Poincaré sections, is shown in Figure 2(l).

5.2. ***Quasiperiodic and chaotic behavior of the impact system in strong resonance cases.*** There exists another route by which Hopf bifurcation leads to chaos in the impact system shown in Figure 1. This route is characterized by a phenomenon in which the system comes into the chaotic motion without a quasi-attracting circle but with a single torus doubling. In order to study such a case, the dynamics of the impact system with system parameters $\mu = 0.04$, $\omega_n = 0.6$, $\zeta = 0.025$, $R = 0.7$, $\delta = 8.0$ is analyzed for $\omega \in [0.93, 0.98]$ by numerical simulation. The dynamic behavior of the system is shown in the projected Poincaré sections; see Figure 4. The eigenvalues of $Df(\omega, 0)$ are computed, and the variation of the eigenvalues is shown in Figure 3(a). When ω decreases through $\omega_c = 0.976327$, a pair of complex conjugate eigenvalues $\lambda_1(\omega_c)$ and $\lambda_2(\omega_c)$ cross the unit circle and all other eigenvalues $\lambda_3(\omega_c)$ and $\lambda_4(\omega_c)$ will still stay inside the unit circle. Then ω_c is a Hopf bifurcation value, and $\lambda_{1,2}(\omega_c) = -0.0000048 \pm 1.000037i$, $\lambda_{1,2}^4(\omega_c) = 1$, $\lambda_{3,4}(\omega_c) = 0.2026327 \pm 0.6311391i$. It is obvious that the model with this set of parameters satisfies the strong resonance condition at the critical point.

Numerical simulation shows that the impact system exhibits an attracting invariant circle in projected Poincaré section for 3561 impacts; see Figure 4(a). It is to be noted that the attracting invariant circle is smooth in nature near the bifurcation point. However, with a further decrease in the control parameter ω, the attracting circle expands and the smoothness of circle is destroyed; see Figure 4(b,c). When $\omega = 0.9454$, the system yields 4-4-4 quasiperiodic impact motion in Figure 4(d). Subsequently, at $\omega = 0.945$, phase locking occurs, and the quasiperiodic motion is locked into the periodic attractors of higher period (than one cycle of the force); see Figure 4(e). With an increase in the control parameter ω, the invariant circle becomes unstable and the system settles into chaotic motion. After the invariant circle loses its stability, no tori doubling or phase locking occurs, and the circle is quasi-attracting (map points inside the circle may be attracted to the circle and map points on or outside the circle may stray from the circle). The chaotic motions of system, represented by "belt-like" attractors in projected Poincaré sections, are shown in Figure 4(f,g), and the width of the belt attractors increases with a decrease in the control parameter. When $\omega = 0.9386$, the chaotic motion of the system grows

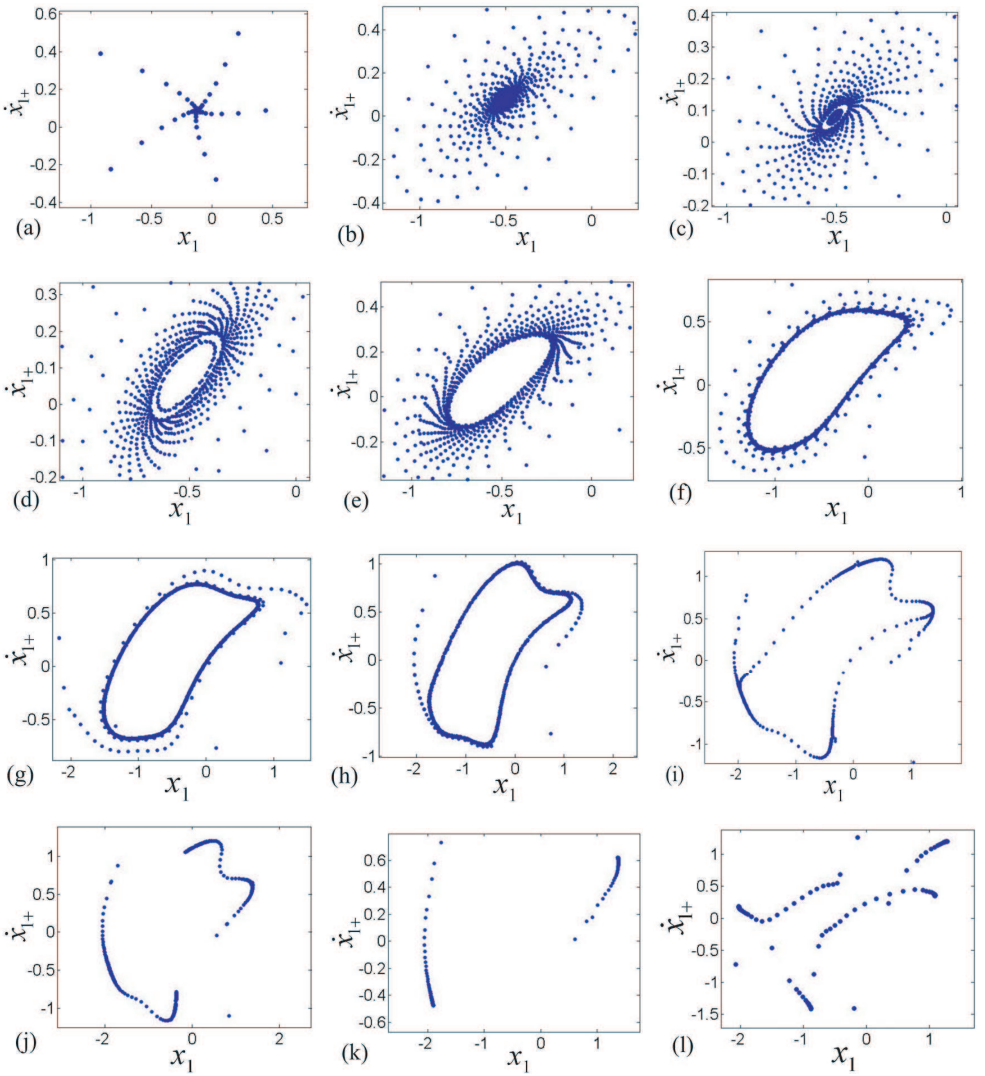

Figure 2. Projected Poincaré mapping section $(x_1, \dot{x}_{1+})$: (a) $\omega = 1.2$, stable 1-1-1 fixed point; (b) $\omega = 1.01962$, stable fixed point; (c) $\omega = 1.0011368$, unstable 1-1-1 fixed point; (d) ω=1.00857, unstable invariant torus; (e) $\omega = 1.00734$, an attracting invariant circle; (f) $\omega = 1.00314$, quasiperiodic 4-4-4 impacts; (g) $\omega = 0.9958$, quasiperiodic impacts; (h) $\omega = 0.99$, quasiperiodic 10-10-10 impact motions; (i) $\omega = 0.98193$, initial break quasiperiodic invariant circle; (j) $\omega = 0.98185$, break of quasiperiodic circle; (k) $\omega = 0.9817$, phase locked; (l) $\omega = 0.970453$, chaotic motions represented by a discontinuous infinite point set.

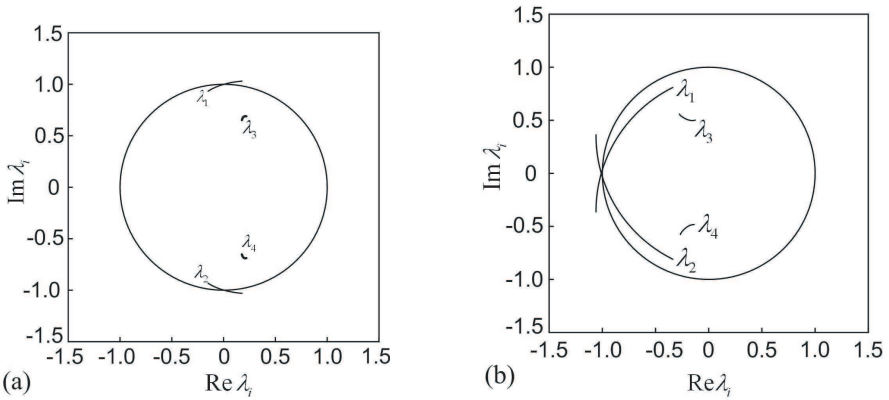

Figure 3. The conjugate pair of eigenvalues intersecting the unit circle for the strong resonance case.

out of the trivial attractor; see Figure 4(h). As the control parameter decreases further, as $\omega = 0.937$, the chaotic motion of the system disappears, and again the system displays a stable 1-1-1 fixed point in projected Poincaré section; see Figure 4(i).

We next study the dynamic behavior of the impact system using numerical simulation, to determine the dynamics near the resonance point ($\lambda_{1,2}^2(\omega_c) = 1$). The system parameters $\mu = 0.05092$, $\zeta = 0.015$, $\omega_n = 1$, $R = 0.7$, $\delta = 6.0$ are chosen. The eigenvalues of $Df(\omega, 0)$ are computed for $\omega \in [0.415, 0.448]$ and two pairs of complex conjugate eigenvalues $\lambda_{1,2}(\omega)$ and $\lambda_{3,4}(\omega)$ are obtained. The conjugate pair of eigenvalues intersecting the unit circle is shown in Figure 3(b). When the control parameter ω decreases to $\omega_c = 0.43186$, the complex conjugate eigenvalues $\lambda_{1,2}(\omega_c)$ intersect the unit circle through the point $(-1, 0)$, and $\lambda_{3,4}(\omega_c)$ remains inside the unit circle. This ω_c is the Hopf bifurcation value, at which $\lambda_{1,2}(\omega_c) = -1.0000031 \pm 0.00000272i$, $\lambda_{1,2}^2(\omega_c) = 1$, $\lambda_{3,4}(\omega_c) = 0.2054234 \pm 0.4398154i$. Numerical simulation results in the projected Poincaré section are shown in Figure 5. After ω passes through the critical value ω_c, the symmetric 1-1-1 periodic impact motion destabilizes, which subsequently leads to a Hopf bifurcation into quasiperiodic motion, as seen in Figure 5(a). When $\omega_c = 0.418$, the smooth attracting invariant circle is destroyed; see Figure 5(b). With a further decrease in ω, after the invariant circle loses its stability, torus doubling and phase locking occur in succession; see Figure 5(c,d). As ω is decreased further, chaotic motion arises: Figure 5(e,f). The evolution from quasiperiodic motion to chaos is clearly shown in the projected Poincaré map in Figure 5. This kind of route from quasiperiodic

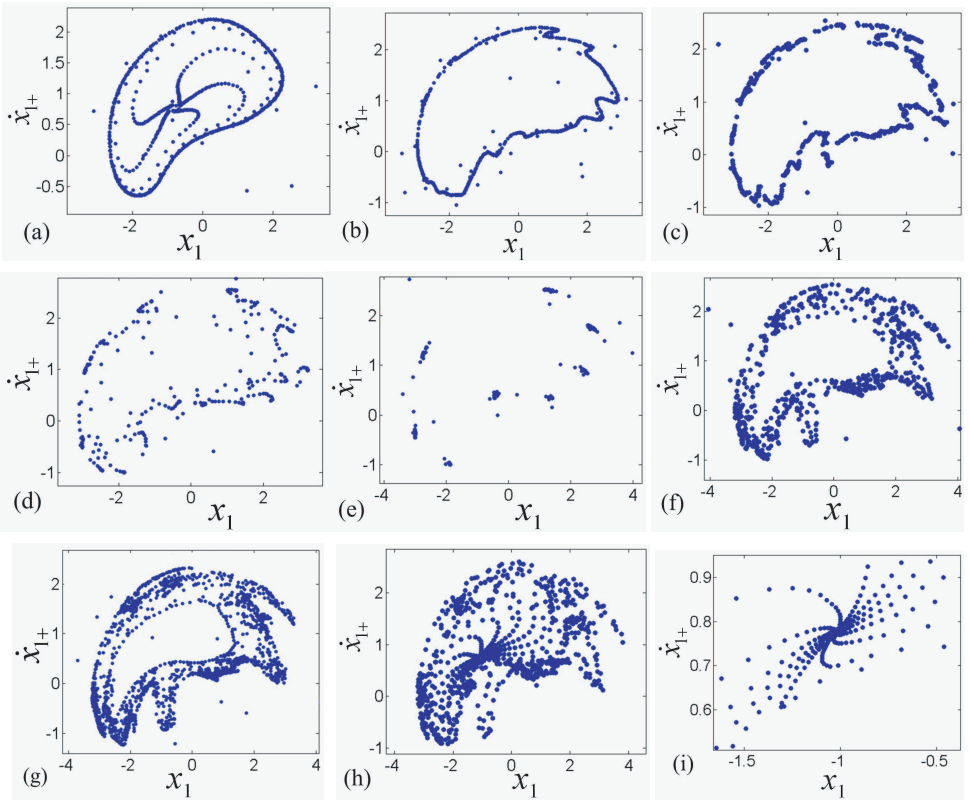

Figure 4. Projected Poincaré section $(x_1, \dot{x}_{1+})$: (a) $\omega = 0.975$, quasiperiodic motion represented by an attracting invariant circle; (b) $\omega = 0.96$, quasiperiodic impacts with wave of oscillation; (c) $\omega = 0.9526$, quasiperiodic impacts; (d) $\omega = 0.9454$, 4-4-4 periodic motion; (e) $\omega = 0.945$, phased locked; (f) $\omega = 0.94$, chaotic motion; (g) $\omega = 0.93998$, chaotic motion; (h) $\omega = 0.9386$, the chaotic motion comes out the trivial attractor; (i) $\omega = 0.937$, stable 1-1-1 fixed point.

impacts to chaos via quasi-attracting invariant circles is often observed in numerical simulations of the dynamics of impact systems.

6. Conclusion

We studied the dynamic behavior of a two-degree-of-freedom impact system via theoretical analysis and numerical simulation. The Poincaré map and fixed point of period 1-1-1 impact are determined analytically. The local dynamical behavior is discussed when the control parameters are changed near the critical point. The

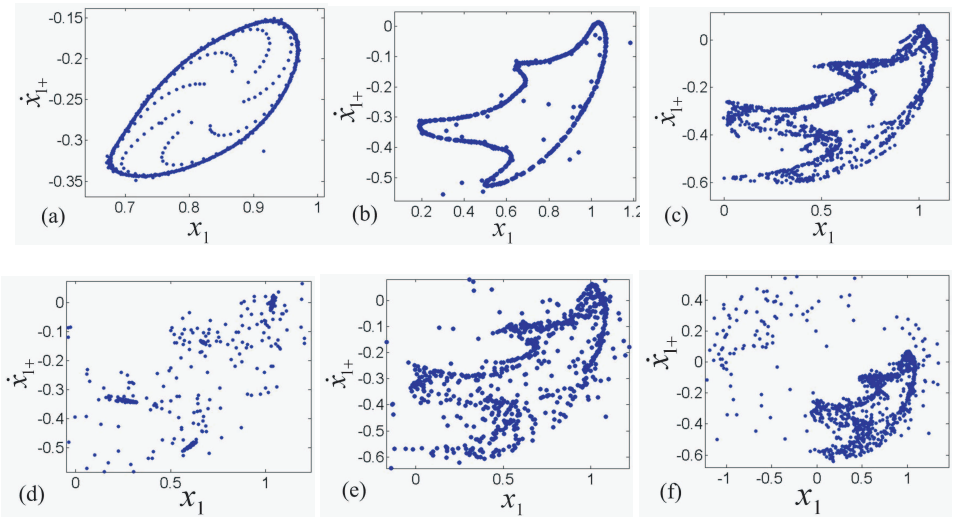

Figure 5. Projected Poincaré section $(x_1, \dot{x}_{1+})$: (a) $\omega = 0.4268$, an attracting invariant circle; (b) $\omega = 0.418$, an attracting invariant circle; (c) $\omega = 0.41754$, the torus doubling; (d) $\omega = 0.41731$, phased locked; (e) $\omega = 0.41721$, chaotic motion; (f) $\omega = 0.41719$, chaotic motion.

dynamic behavior of the system in the strong resonance case is more complicated than in nonresonance and weak resonance cases. In the strong resonance case $\lambda_{1,2}^4(\omega_c) = 1$, the system can exhibit stable 4-4-4 periodic impact motion and quasiperiodic motion, and the route from quasiperiodic motion to chaos is observed by numerical simulation. In the strong resonance cases of $\lambda_{1,2}^2(\omega_c) = 1$, the system transitions from quasiperiodic impacts to chaos in a complicated way: quasiperiodic impacts $\rightarrow$ torus doubling $\rightarrow$ various kinds of phase locking $\rightarrow$ chaos. The method established in the paper can be extended to some other analogous systems. Machines and equipment whose behavior can be attempted to be modeled sy such systems include vibration hammers, gear transmission, shakers, wheel-rail interaction of high-speed coaches, and compacting machinery. However, it is necessary to make further theoretical studies of the routes of bifurcation to chaos.

Appendix

The relational coefficients are shown as follows:

$$g_{11}=\frac{1}{4}\left[\frac{\partial^2 F_1}{\partial y_1^2}+\frac{\partial^2 F_1}{\partial y_2^2}+i\left(\frac{\partial^2 F_2}{\partial y_1^2}+\frac{\partial^2 F_2}{\partial y_2^2}\right)\right] \tag{A1}$$

$$g_{02}=\frac{1}{4}\left[\frac{\partial^2 F_1}{\partial y_1^2}-\frac{\partial^2 F_1}{\partial y_2^2}-2\frac{\partial^2 F_2}{\partial y_1\partial y_2}+i\left(\frac{\partial^2 F_2}{\partial y_1^2}-\frac{\partial^2 F_2}{\partial y_2^2}+2\frac{\partial^2 F_1}{\partial y_1\partial y_2}\right)\right] \tag{A2}$$

$$g_{20}=\frac{1}{4}\left[\frac{\partial^2 F_1}{\partial y_1^2}-\frac{\partial^2 F_1}{\partial y_2^2}+2\frac{\partial^2 F_2}{\partial y_1\partial y_2}+i\left(\frac{\partial^2 F_2}{\partial y_1^2}-\frac{\partial^2 F_2}{\partial y_2^2}-2\frac{\partial^2 F_1}{\partial y_1\partial y_2}\right)\right] \tag{A3}$$

$$g_{21}=G_{21}+\sum_{i=1}^{n-2}\left(2G_{10}^s w_{11}^s+G_{01}^s w_{20}^s\right) \tag{A4}$$

$$\begin{aligned}G_{21}=\frac{1}{8}\Bigg[&\frac{\partial^3 F_1}{\partial y_1^3}+\frac{\partial^3 F_1}{\partial y_1\partial y_2^2}+\frac{\partial^3 F_2}{\partial y_1^2\partial y_2}+\frac{\partial^3 F_2}{\partial y_2^3}\\&+i\left(\frac{\partial^3 F_2}{\partial y_1^3}+\frac{\partial^3 F_2}{\partial y_1\partial y_2^2}-\frac{\partial^3 F_1}{\partial y_1^2\partial y_2}-\frac{\partial^3 F_1}{\partial y_2^3}\right)\Bigg]\end{aligned} \tag{A5}$$

$$G_{10}^{k-2}=\frac{1}{2}\left[\frac{\partial^2 F_1}{\partial y_1\partial y_k}+\frac{\partial^3 F_2}{\partial y_2\partial y_k}+i\left(\frac{\partial^2 F_2}{\partial y_1\partial y_k}-\frac{\partial^3 F_1}{\partial y_2\partial y_k}\right)\right](k=3,\ldots,n) \tag{A6}$$

$$G_{01}^{k-2}=\frac{1}{2}\left[\frac{\partial^2 F_1}{\partial y_1\partial y_k}-\frac{\partial^3 F_2}{\partial y_2\partial y_k}+i\left(\frac{\partial^2 F_2}{\partial y_1\partial y_k}-\frac{\partial^3 F_1}{\partial y_2\partial y_k}\right)\right](k=3,\ldots,n) \tag{A7}$$

$$W_{11}=(I-B)^{-1}H_{11},\qquad W_{02}=\left(\bar{\lambda}^2 I-B\right)^{-1}H_{02}, \tag{A8}$$

where $W_{11}=(w_{11}^1, w_{11}^2,\ldots,w_{11}^{n-2})^T$, $W_{02}=(w_{02}^1, w_{02}^2,\ldots,w_{02}^{n-2})^T$.

$$H_{11}^{k-2}=\frac{1}{4}\left(\frac{\partial^2 F_k}{\partial y_1^2}+\frac{\partial^2 F_k}{\partial y_2^2}\right)\ (k=3,4) \tag{A9}$$

$$H_{02}^{k-2}=\frac{1}{4}\left(\frac{\partial^2 F_k}{\partial y_1^2}-\frac{\partial^2 F_k}{\partial y_2^2}-2i\frac{\partial^2 F_k}{\partial y_1\partial y_2}\right)\ (k=3,4) \tag{A10}$$

References

[Asfar and Akour 2005] K. R. Asfar and S. N. Akour, "Optimization analysis of impact viscous damper for controlling self-excited vibrations", *J. Vib. Control* **11**:1 (2005), 103–120.

[di Bernardo et al. 2001] M. di Bernardo, C. J. Budd, and A. R. Champneys, "Normal form maps for grazing bifurcations in n-dimensional piecewise-smooth dynamical systems", *Phys. D: Nonlinear Phenom.* **160**:3-4 (2001), 222–254. MR 2002k:37084

[di Bernardo et al. 2002] M. di Bernardo, P. Kowalczyk, and A. Nordmark, "Bifurcations of dynamical systems with sliding: derivation of normal-form mappings", *Phys. D: Nonlinear Phenom.* **170**:3-4 (2002), 175–205. MR 2003h:37075

[Blazejczyk-Okolewska 2001] B. Blazejczyk-Okolewska, "Analysis of an impact damper of vibrations", *Chaos Solitons Fract.* **12**:11 (2001), 1983–1988.

[Budd et al. 1995] C. Budd, F. Dux, and A. Cliffe, "The effect of frequency and clearance variations on single-degree-of-freedom impact oscillators", *J. Sound Vib.* **184**:3 (1995), 475–502.

[Chatterjee and Mallik 1995] S. Chatterjee and A. Mallik, A. K.and Ghosh, "On impact dampers for non-linear vibrating systems", *J. Sound Vib.* **187**:3 (1995), 403–420.

[Chatterjee and Mallik 1996] S. Chatterjee and A. K. Mallik, "Bifurcations and chaos in autonomous self-excited oscillators with impact damping", *J. Sound Vib.* **191**:4 (1996), 539–562. MR 97f:70049

[Cheng and Wang 2003] C. C. Cheng and J. Y. Wang, "Free vibration analysis of a resilient impact damper", *Int. J. Mech. Sci.* **45**:4 (2003), 589–604.

[Cone and Zadoks 1995] K. M. Cone and R. I. Zadoks, "A numerical study of an impact oscillator with the addition of dry friction", *J. Sound Vib.* **188**:5 (1995), 659–683.

[Dimentberg and Iourtchenko 2004] M. F. Dimentberg and D. V. Iourtchenko, "Random vibrations with impacts: a review", *Nonlinear Dyn.* **36**:2-4 (2004), 229–254. MR 2005c:74038

[Ding et al. 2004] W. C. Ding, J. H. Xie, and Q. S. Sun, "Interaction of Hopf and period doubling bifurcations of a vibro-impact system", *J. Sound Vib.* **275**:1-2 (2004), 27–45.

[Ema and Marui 1996] S. Ema and E. Marui, "Damping characteristics of an impact damper and its application", *Int. J. Mach. Tools Manuf.* **36**:3 (1996), 293–306.

[Holmes 1982] P. J. Holmes, "The dynamics of repeated impacts with a sinusoidally vibrating table", *J. Sound Vib.* **84**:2 (1982), 173–189. Erratum in **88**:2 (1983), 287. MR 676219 (85f:70044a) Zbl 0518.73015

[Lanford 1973] O. E. Lanford, "Bifurcation of periodic solutions into invariant tori: the work of Ruelle and Takens", pp. 159–192 in *Nonlinear problems in the physical sciences and biology* (Seattle, 1972), edited by I. Stakgold et al., Lecture Notes in Mathematics **322**, Springer, Berlin, 1973. MR 0371548 (51 #7766)

[Luo 2004a] A. C. J. Luo, "Period-doubling induced chaotic motion in the LR model of a horizontal impact oscillator", *Chaos Solitons Fract.* **19**:4 (2004), 823–839. MR MR2009668

[Luo 2004b] G. W. Luo, "Period-doubling bifurcations and routes to chaos of the vibratory systems contacting stops", *Phys. Lett. A* **323**:3-4 (2004), 210–217. MR 2050484

[Luo and Chen 2005] A. C. J. Luo and L. Chen, "Periodic motions and grazing in a harmonically forced, piecewise, linear oscillator with impacts", *Chaos Solitons Fract.* **24**:2 (2005), 567–578.

[Luo and Xie 2003] G. W. Luo and J. H. Xie, "Codimension two bifurcation of periodic vibro-impact and chaos of a dual component system", *Phys. Lett. A* **313**:4 (2003), 267–273. MR 1995513

[Luo et al. 2001] G. W. Luo, J. H. Xie, and H. L. Guo, "Periodic motions and global bifurcations of a two-degree-of-freedom system with plastic vibro-impact", *J. Sound Vib.* **240**:5 (2001), 837–858.

[Nordmark 1991] A. B. Nordmark, "Non-periodic motion caused by grazing incidence in an impact oscillator", *J. Sound Vib.* **145**:2 (1991), 279–297.

[Padmanabhan and Singh 1995] C. Padmanabhan and R. Singh, "Analysis of periodically excited non-linear systems by a parametric continuation technique", *J. Sound Vib.* **184**:1 (1995), 35–58.

[Shaw and Holmes 1983] S. W. Shaw and P. Holmes, "Periodically forced linear oscillator with impacts: chaos and long-period motions", *Phys. Rev. Lett.* **51**:8 (1983), 623–626. MR 84k:58171

[Thompson and Ghaffari 1982] J. M. T. Thompson and R. Ghaffari, "Chaos after period-doubling bifurcations in the resonance of an impact oscillator", *Phys. Lett. A* **91**:1 (1982), 5–8. MR 83k:70028

[Wan 1978] Y. H. Wan, "Computation of the stability condition for the Hopf bifurcation of diffeomorphisms on R^2", *SIAM J. Appl. Math.* **34**:1 (1978), 167–175. MR 57 #7684

[Wang et al. 2003] J. F. Wang, C. C. Lin, and B. L. Chen, "Vibration suppression for high-speed railway bridges using tuned mass dampers", *Int. J. Solids Struct.* **40**:2 (2003), 465–491.

[Wen 2001] G. L. Wen, "Codimension-2 Hopf bifurcation of a two-degree-of-freedom vibro-impact system", *J. Sound Vib.* **242**:3 (2001), 475–485.

[Whiston 1992] G. S. Whiston, "Singularities in vibro-impact dynamics", *J. Sound Vib.* **152**:3 (1992), 427–460. MR 92m:58080

[Xie and Ding 2005] J. Xie and W. Ding, "Hopf-Hopf bifurcation and invariant torus $\mathbf{T}^2$ of a vibro-impact system", *Int. J. Non-Linear Mech.* **40**:4 (2005), 531–543. MR 2005j:70052

Received 22 Sep 2005. Revised 17 Nov 2005.

JIANLIAN CHENG: cheng19690912@163.com
Department of Engineering Mechanics, MOE Key Laboratory for Strength and Vibration, School of Aerospace, Xi'an Jiaotong University, Xi'an 710049, China

HUI XU: xuhui@mail.xjtu.edu.cn
Department of Engineering Mechanics, MOE Key Laboratory for Strength and Vibration, School of Aerospace, Xi'an Jiaotong University, Xi'an 710049, China